Journal of Power Sources 208 (2012) 52–57

Contents lists available at SciVerse ScienceDirect

Journal of Power Sources

journal homepage: www.elsevier.com/locate/jpowsour

Calendering effects on the physical and electrochemical properties of $Li[Ni_{1/3}Mn_{1/3}Co_{1/3}]O_2$ cathode

Honghe Zheng[a,b,*], Li Tan[a], Gao Liu[b], Xiangyun Song[b], Vincent S. Battaglia[b]

[a] School of Energy, Soochow University, Suzhou, Jiangsu 215006, China
[b] Lawrence Berkeley National Laboratory, 1 Cyclotron Rd, Berkeley, CA 94720, USA

ARTICLE INFO

Article history:
Received 19 September 2011
Received in revised form
27 December 2011
Accepted 1 February 2012
Available online 14 February 2012

Keywords:
Lithium ion batteries
Cathode
Porosity
Rate capability
Activation energy

ABSTRACT

$Li[Ni_{1/3}Mn_{1/3}Co_{1/3}]O_2$ cathode laminate containing 8% PVDF and 7% acetylene black is fabricated and calendered to different porosities. Calendering effects on the physical and electrochemical properties of the $Li[Ni_{1/3}Mn_{1/3}Co_{1/3}]O_2$ cathode are investigated. It is found that mechanical properties of the composite laminate strongly depend on the electrode porosity whereas the electronic conductivity is not significantly affected by calendering. Electrochemical performances including the specific capacity, the first coulombic efficiency, cycling performance and rate capability for the cathode at different porosities are compared. An optimized porosity of around 30–40% is identified. Electrochemical impedance spectroscopy (EIS) studies illustrate that calendering improves the electronic conductivity between active particles at relatively high porosities, but increases charge transfer resistance at electrode/electrolyte interface at relatively low porosities. An increase of activation energy of Li interfacial transfer for the electrode at 0% porosity indicates a relatively high barrier of activation at the electrode/electrolyte interface, which accounts for the poor rate capability of the electrode at extremely low porosity.

1. Introduction

In the production of lithium ion batteries, calendering is an indispensable step used to press an electrode and typically performed after the electrode casting and drying steps [1,2]. Calendering is believed to be important for it improves particle-to-particle contact within the electrode and enhances the adhesion between the electrode and the current collector. Pressing an electrode also contributes to improvement of volumetric energy density due to the decrease of electrode thickness at the same active material loading. Seen from all these points, calendering is helpful enhancing the physical and electrochemical properties of an electrode. However, porosity decrease of the electrode aroused from calendering reduces the specific area of the electrode and increases the electrode tortuosity as well. Li migration within the electrode of low porosity may be hindered. Therefore, calendering an electrode down to an optimized porosity is very crucial for the production of electrode laminate of high electrochemical performance [3,4]. However, the present case is that the calendering process is still empirical in lithium ion battery industries. Investigation of calendering effects on the physical and electrochemical performance helps to design and optimize electrode logically.

In this study, a layered transition metal oxide, $Li[Ni_{1/3}Co_{1/3}Mn_{1/3}]O_2$, is employed as the cathode material. This kind of cathode material is developing rapidly and of great potential use in 3C market (computer, communication and consumer electronics) [5,6]. Compared with other commonly used cathode materials such as $LiCoO_2$, $LiMn_2O_4$, and $LiFePO_4$, etc., $Li[Ni_{1/3}Co_{1/3}Mn_{1/3}]O_2$ offers advantages of high energy density, high power density, satisfactory cycling capability and good thermal stability at fully charged state. Therefore, it is widely accepted to be promising for lithium-ion batteries for electric vehicle (EV) and hybrid electric vehicle (HEV) applications [7,8]. In the development of lithium ion batteries based on the $Li[Ni_{1/3}Co_{1/3}Mn_{1/3}]O_2$ cathode, much attention has been paid to the fabrication and optimization of the material itself. Technologies involved in the electrode preparation and optimization are of great significance to meet EV and HEV requirements, which has not been subject to in-depth studies so far.

The purpose of this study is to investigate the calendering effects on the physical and electrochemical properties of the $Li[Ni_{1/3}Co_{1/3}Mn_{1/3}]O_2$ cathode containing commonly used amount of poly(vinylidene difluoride) (PVDF) binder and acetylene black (AB) conductive additive. An optimized porosity for the electrode in terms of the specific capacity, the first coulombic efficiency and rate capability is identified. The reasons associated with the

* Corresponding author at: School of Energy, Soochow University, Suzhou, Jiangsu 215006, China. Tel.: +86 512 69153523; fax: +86 512 67870271.
E-mail address: hhzheng66@yahoo.com.cn (H. Zheng).

0378-7753/$ – see front matter © 2012 Elsevier B.V. All rights reserved.
doi:10.1016/j.jpowsour.2012.02.001

Table 1
The real thicknesses of the electrode at different porosities.

Electrode thickness (μm)	Real porosity (%)	Desired porosity (%)
188	49.5	50%
161	40.7	40%
137	29.2	30%
124	20.3	20%
119	9.0	10%
100	0.3	0%

physical and electrochemical property changes are discussed. The results obtained in this study may shed new light on the design of cathode laminate for EV and HEV applications.

2. Experimental

A commercial $Li[Ni_{1/3}Co_{1/3}Mn_{1/3}]O_2$ active material was obtained from Seimi Co, USA. Slurries consisting of 8% PVDF binder, 7% acetylene black, and 85% $Li[Ni_{1/3}Co_{1/3}Mn_{1/3}]O_2$ in a certain amount of 1-methyl-2-pyrrolidone (NMP) solvent were prepared by mechanical mixing at 4000 rpm for 2 h. This recipe is very typical in lithium ion battery industries for production of $Li[Ni_{1/3}Co_{1/3}Mn_{1/3}]O_2$ laminate. The cathode film was cast on aluminum foil by using a doctor blade method. In order to clearly observe the calendering effects, the loading of active material was controlled at around 30 mg cm^{-2}, around 3 times as high as the commercial products.

Porosity of the electrode was calculated taking into account of the true density of the mix obtained from X-ray measurements according to the following equation [9].

$$\text{porosity} = \frac{L - W((C1/D1) + (C2/D2) + (C3/D3))}{L} \quad (1)$$

where L is the real thickness of the electrode laminate (without Al foil), W is the weight of the laminate per area, $C1$, $C2$, and $C3$ are the percentage of active material, PVDF binder and acetylene black within the electrode laminate while $D1$, $D2$, and $D3$ are the true density for $Li[Ni_{1/3}Co_{1/3}Mn_{1/3}]O_2$, PVDF and acetylene black, respectively. The true densities for $Li[Ni_{1/3}Co_{1/3}Mn_{1/3}]O_2$ active material, PVDF and acetylene black are 4.68, 1.78, and 1.95 g cm^{-3}, respectively. The cast and dried films had a free-standing porosity of around 50%. All the porosities were calculated by assuming that the weight fractions and density of each material were not changed by the fabrication process.

During the calendering process, a section of electrode laminate was fed through the gap of the milling machine to compress the electrode to a desired thickness corresponding to the desired electrode porosity. The electrode porosities were adjusted from free standing to 40%, 30%, 20%, 10%, and 0%; respectively. Variation of the porosity was controlled within ±1%. The real thicknesses of the electrode at different porosities are listed in Table 1.

After being calendered to different porosities, 2.5 cm × 5 cm sections were cut out and the laminates were removed from the aluminum current collectors. Mechanical properties of the laminate were determined by using a Chatillon TCD225 force measurement system. The schematic of the mechanical experiment setup to determine breaking strength and Young's modulus of the electrode laminate at different porosities is shown in Fig. 1. A stretching speed of 0.00127 mm s^{-1} was applied in this study. Determination for each sample was repeated for at least 5 times. Breaking stress is defined as the quotient of the maximum force applied onto the film till it breaks and the section area of the laminate. It is calculated from the following equation:

$$\text{breaking stress} = \frac{\text{force}_{\max}}{\text{width} \times \text{thickness}} \quad (2)$$

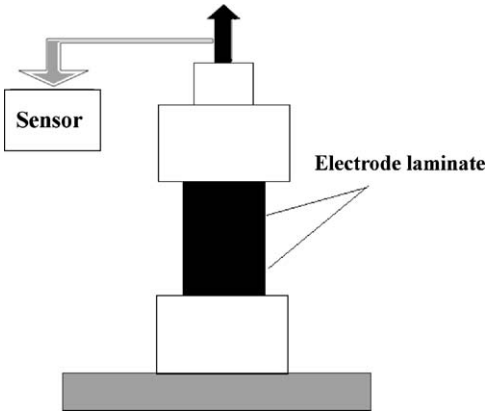

Fig. 1. Schematic of the mechanical experiment setup used to determine the tensile strength and Young's modulus of the cathode laminate.

Strain is the ratio of change in length (ΔL) vs. the initial length (L) of the laminate:

$$\text{strain} = \frac{\Delta L}{L} \quad (3)$$

Young's modulus (E) is the gradient of stress vs. strain function:

$$E = \frac{\text{stress}}{\text{strain}} = \text{stress} \times \frac{L}{\Delta L} \quad (4)$$

The electronic conductivity of the laminate was determined with a four-point probe (RM3-AR) test unit from JANDEL (UK). The measurements were taken on the electrode films removed from the aluminum, and placed on a non-conducting glass substrate. A Hitachi S-4700 scanning electron microscope (SEM) operating at 200 kV was used to view the morphologies of the electrode at different porosities.

The rest electrode at different porosities was punched into discs of 12.7 mm diameter and subject to thorough drying for 16 h at 130 °C under vacuum. Coin cells were assembled in an argon-filled glove box (dew point ≤ −80 °C). Lithium foil was used as the counter electrode and Celgard 2400 was used as the separator. 1 mol dm^{-3} $LiPF_6$/EC + DEC (1:1) from Novolyte was used as the electrolyte. All cells were tested at 303 K on a Maccor battery cycler. Three formation cycles at C/10 charge and discharge were first applied. The upper charge voltage limit was set at 4.5 V and the discharge voltage limit was set at 3.0 V vs. Li/Li^+. Cycling test for the cathode at different porosities was carried out at C/10 charge and discharge for 25 cycles. Rate performance of the cathode at different porosities was measured following the formation cycles. The discharge capacity determined from the last formation was used to estimate the C-rate for all subsequent cycles for each cell. The rate performance test consisted of full discharges at rates of C/10, C/5, C/2, 1C, 2C, 5C, and 10C, down to 3.0 V. A charge of C/10 to 4.5 V preceded each discharge.

The impedance spectra (100 kHz to 10 mHz, 5 mV perturbation) of the cathodes were recorded using a Solartron 1286 with a three-electrode Swagelok cell that included a lithium counter and reference electrode. The measurements were performed after the cell was completely formed and charged to a potential of 4.2 V vs. Li/Li^+. Each electrode was held at 4.2 V and under a certain temperature for at least 3 h to attain a condition of sufficiently low residual current and temperature equilibrium. To avoid side reactions possibly occurred at electrode/electrolyte interface under high temperature, the temperature was varied from −15 to 30 °C with a precision of ±0.5 °C for each temperature.

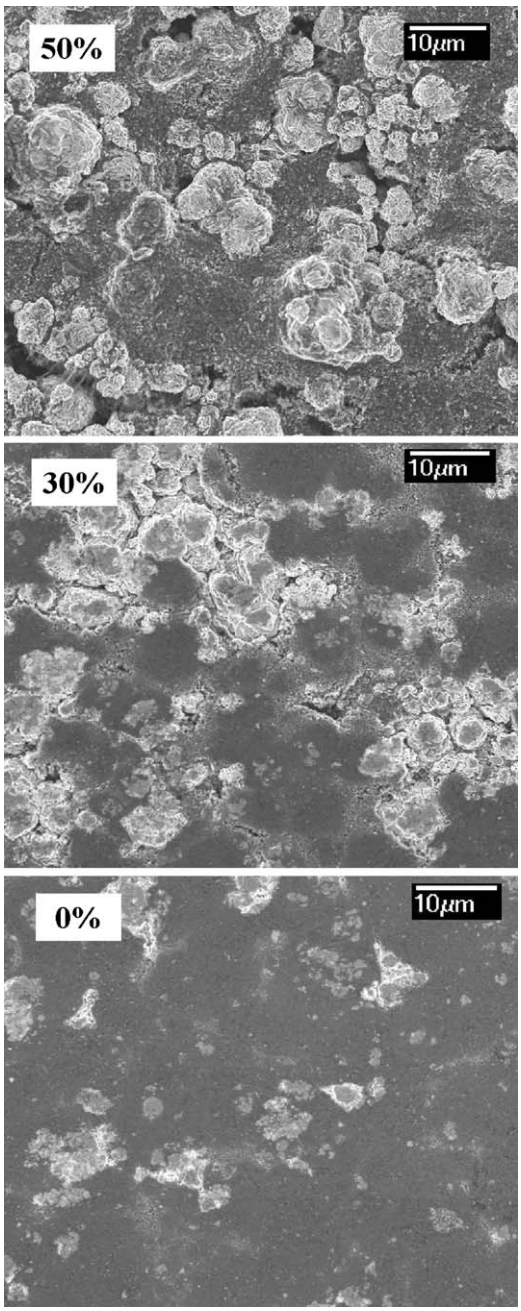

Fig. 2. SEM images of the $Li[Ni_{1/3}Mn_{1/3}Co_{1/3}]O_2$ cathode containing 8% PVDF, 7% acetylene black at different porosities.

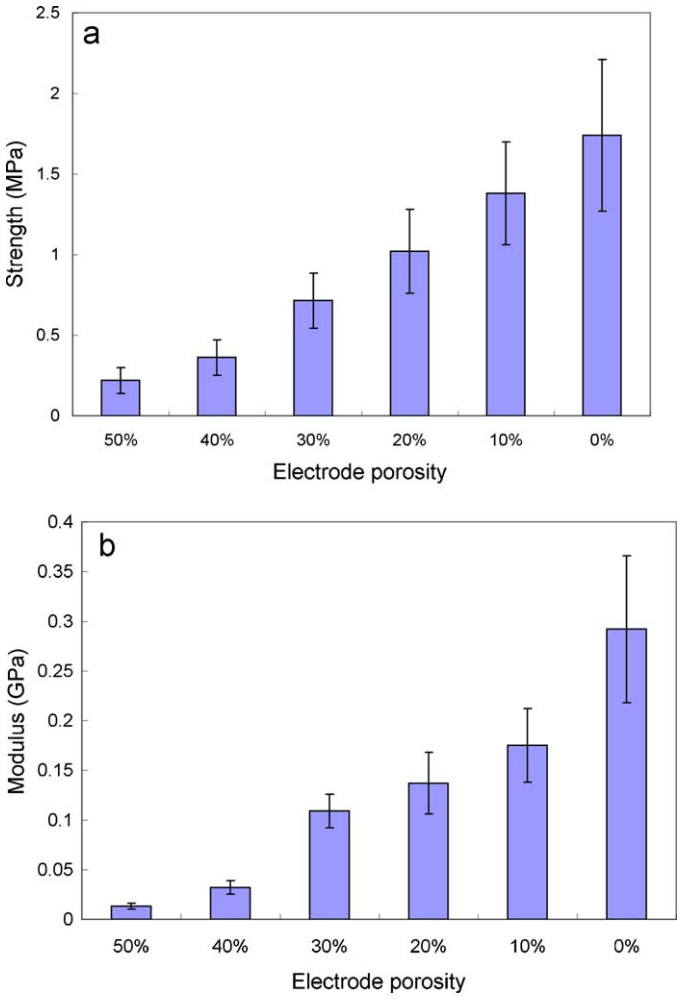

Fig. 3. Variations of breaking stress (a) and Young's modulus (b) of the $Li[Ni_{1/3}Co_{1/3}Mn_{1/3}]O_2$ cathode laminate with the electrode porosities.

3. Results and discussion

Morphologies of the $Li[Ni_{1/3}Co_{1/3}Mn_{1/3}]O_2$ cathode containing 8% PVDF and 7% acetylene black at three different porosities, free standing (50%), 30%, and 0%, are shown in Fig. 2. For the free standing laminate sample, lots of pores and micro-fractures are observed throughout the electrode. The composite of PVDF binder and acetylene black distributed in between active material particles looks very loose. The inactive materials take a large volume fraction of the electrode. The electrode of high porosity can soak a large fraction of electrolyte within a cell. Therefore, the volumetric energy density of the electrode is low due to low volumetric fraction of the active material. At 30% porosity, morphology of the inactive material composite (binder and acetylene black mixture) is greatly changed. The inactive material composite seems to be quite dense. As the active material is not deformed or crashed by calendering, the decrease of the electrode thickness is attributed mainly to the shrinkage of the inactive material composite. The distance between neighboring active particles is reduced with the decrease of the electrode thickness. The volumetric energy density can thus be improved due to the increase of volumetric fraction of the active material. By contrast, compression of the electrode to the calculated 0% porosity thickness, the inactive material composite seems to be more dense and almost all the open pores and fractures are eliminated. Nevertheless, there is still some small observable open space within the laminates. This is because the porosity was calculated based on the assumption that no lateral expansion of the laminate or the aluminum current collector occurs during the calendering process.

Morphological change of the electrode will inevitably bring about some physical property change of the laminate. Variation of mechanical properties including breaking stress and Young's modulus (E) of the cathode laminate with electrode porosities is displayed in Fig. 3. As shown in Fig. 3a, the breaking stress of the $Li[Ni_{1/3}Mn_{1/3}Co_{1/3}]O_2$ laminate increases with decreasing porosity of the electrode. This result can be explained by the morphological change of the composite laminate. At high porosity, not only the inactive material composite is seen very loose, the combination between inactive and active materials is also very weak. Many pores and fractures are observed throughout the electrode. The laminate is very easy to break when subject to stretch. Calendering squeezes the inactive materials together and improves the adhesion between

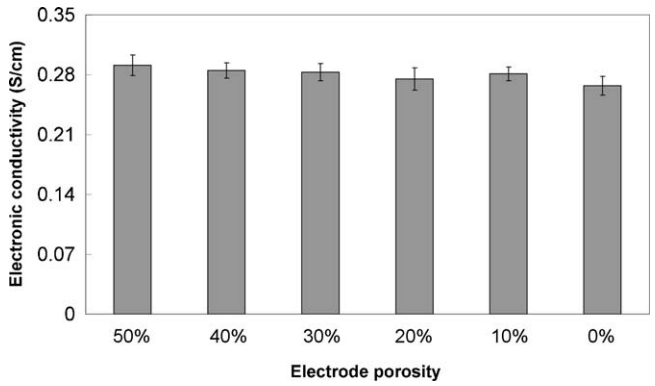

Fig. 4. Electronic conductivities of the $Li[Ni_{1/3}Mn_{1/3}Co_{1/3}]O_2$ laminate at different porosities.

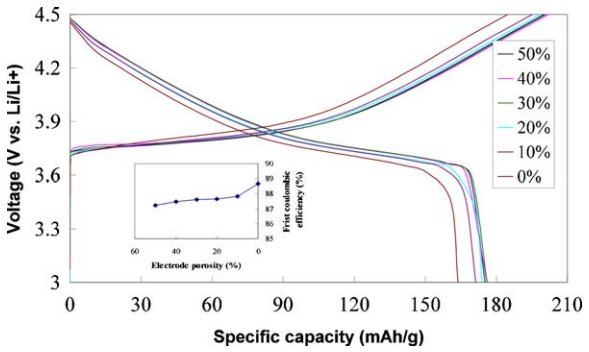

Fig. 5. The first charge–discharge profiles of the $Li[Ni_{1/3}Mn_{1/3}Co_{1/3}]O_2$ cathode at different porosities.

the inactive material composite and active material particles. The strength of the laminate is thus increased. The increase of breaking stress illustrates that the active material particles are held together more effectively and the electrode is more compact. An electrode of high breaking strength is desirable as it can avoid the shedding of active materials during battery processing and electrochemical cycling. Meanwhile, Young's modulus of the cathode laminate with decreasing porosity is also increased as seen in Fig. 3b. The increase of Young's modulus with caledering seems to be much more rapidly than that of the breaking strength. In physical sense, high Young's modulus implies less elasticity of the laminate. It is not desired for an electrode of high quality. As the active particles contract and expand during Li de-insertion and insertion process, high internal stress is induced during electrochemical cycles for the electrode of high Young's modulus. The high internal stress may bring about structural destruction of the laminate, such as crack or fatigue fracture generation and propagation, which may result in electrochemical deterioration of the electrode. Therefore, there is a compromise between high breaking stress and low Young's modulus for the electrode when subject to calendering.

Electronic conductivity of an electrode laminate is a factor of the electrode resistance during electrochemical cycles [10,11]. A good electrode laminate must have satisfactory electronic conductivity. Generally, it is believed that, if the electronic conductivity is higher than the ionic conductivity of the electrode and the electrolyte, the electronic conductivity will not have much impact on the cells overall impedance. Fig. 4 demonstrates the electronic conductivity of the $Li[Ni_{1/3}Mn_{1/3}Co_{1/3}]O_2$ laminate at different porosities as measured with a four point probe technique. The electronic conductivity of the $Li[Ni_{1/3}Mn_{1/3}Co_{1/3}]O_2$ laminate at different porosities is obtained to be around $0.28\,S\,cm^{-1}$ and the value is not considerably changed by calendering. It is therefore concluded that calendering does not contribute much to the electronic conductivity for the $Li[Ni_{1/3}Mn_{1/3}Co_{1/3}]O_2$ laminate. The electronic conductivity obtained here is significantly higher than the ionic conductivity of the organic electrolyte (around $0.01\,S\,cm^{-1}$) used in this study [12,13]. This means that electronic resistance of the composite electrode is not an important factor affecting the overall impedance within a cell.

Charge–discharge profiles of the $Li[Ni_{1/3}Mn_{1/3}Co_{1/3}]O_2$ electrode at 0.1C under room temperature (30 °C) are demonstrated in Fig. 5. It is seen that calendering affects reversible capacity of the $Li[Ni_{1/3}Mn_{1/3}Co_{1/3}]O_2$ cathode to a certain extent. For the electrode at 20–50% porosity, a reversible capacity of ca. $175\,mAh\,g^{-1}$ was obtained. The specific capacity is not affected by calendering in the porosity range. However, the reversible capacity was considerably decreased when the electrode was pressed down to less than 10% porosity. Around 10% capacity decrease of the electrode was obtained at 0% porosity compared with the electrode at 30% porosity. One reason for the specific capacity decrease at extremely low porosity is ascribed to the poor wettability of the electrode with electrolyte. Some of the active material may not be wet with electrolyte and are electrochemically inert during charge–discharge cycles. The other one reason may be associated with the high electrode impedance aroused from calendaring, which will be discussed next.

The first coulombic efficiency is also an important criterion evaluating the quality of an electrode since high electrochemical efficiency corresponds to less Li consumption during electrochemical cycles. Here we see a slight increase of the first coulombic efficiency with decreasing electrode porosity from 50% down to 0%. The coulombic efficiency rise should be related to the decrease of the specific area of the electrode. For many Li storage materials, the intensity of SEI (solid electrolyte interphase) formation reactions occurred at electrode/electrolyte interface is proportional with the specific area of the electrode under a certain condition. Decrease of the SEI formation reactions due to the low specific surface area of the electrode resulted from calendaring explains the increased first coulombic efficiency at lower porosities.

Here we see another compromise between the specific capacity and the first coulombic efficiency. For an electrode laminate of high quality, both high specific capacity and high coulombic efficiency are preferred. At extremely low porosity, an improvement of the first coulombic efficiency is accompanied by a decrease of the specific capacity. Therefore, calendering must be carefully controlled so as to obtain an optimized porosity of the electrode.

Cycling performance of the $Li[Ni_{1/3}Mn_{1/3}Co_{1/3}]O_2$ cathode at different porosities in $1\,mol\,dm^{-3}$ $LiPF_6$/EC + DEC (1:1) electrolyte is displayed in Fig. 6. As can be distinguished from the 25 cycles, a very identical cycling behavior was obtained. After 25 electrochemical cycles, the electrode lost no more than 5% of its initial capacity, showing a satisfactory cycling capability of the material adopted in this study. The small effect of the electrode porosity on the cycleability is associated with the small volume change (less than 3%) for $Li[Ni_{1/3}Mn_{1/3}Co_{1/3}]O_2$ during Li insertion and extraction.

Rate capability of the $Li[Ni_{1/3}Mn_{1/3}Co_{1/3}]O_2$ electrode at different porosities is shown in Fig. 7. As shown in this figure, a drop off of specific capacity to varying degrees between C/5 and C/2 is observed. The rate performance of the $Li[Ni_{1/3}Mn_{1/3}Co_{1/3}]O_2$ electrodes obtained in this study seems to be worse than those reported results [7.8]. This is due to the high active material loading of the electrode. The $30\,mg\,cm^{-2}$ loading of active material is about 3 times as high as those commercial $Li[Ni_{1/3}Co_{1/3}Mn_{1/3}]O_2$ cathode laminates. It is reported that rate capability deteriorates dramatically with increasing active material loading. A power-law relationship has been developed between rate capability and electrode active material loading for $LiFePO_4$ cathode [14]. However,

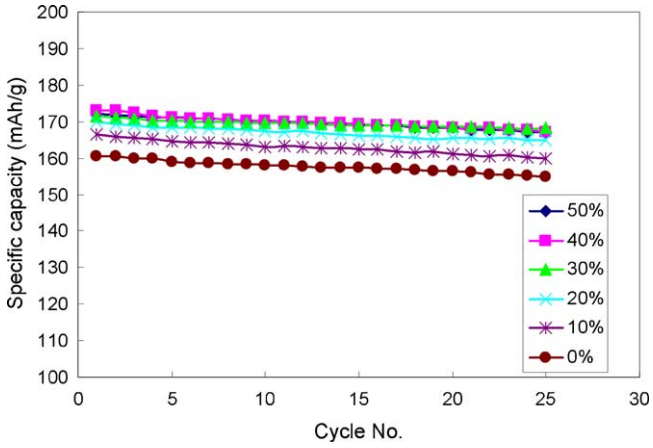

Fig. 6. Cycling performance of the $Li[Ni_{1/3}Mn_{1/3}Co_{1/3}]O_2$ cathode at different porosities in 1.0 M $LiPF_6$/EC + DEC(1:1) electrolyte at 0.1C charge and discharge.

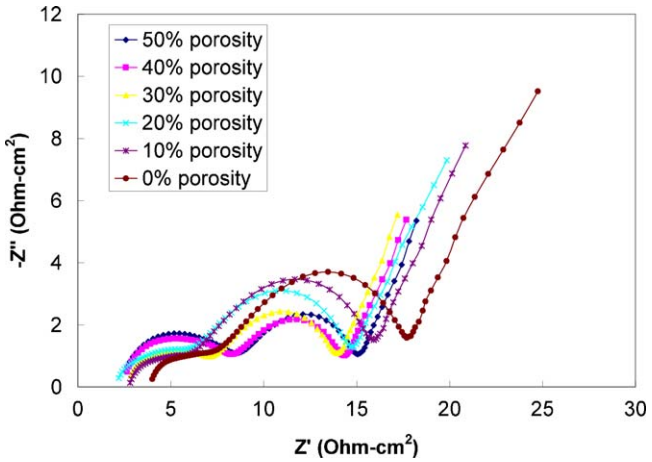

Fig. 8. Nyquist plots of the $Li[Ni_{1/3}Mn_{1/3}Co_{1/3}]O_2$ cathode at different porosities at 4.2 V vs. Li/Li^+ under room temperature.

with high active material loading, we can clearly observe the calendering effect on the rate performance of the electrode.

For the electrode at 30–50% porosity, a comparable rate capability behavior is obtained. It is seen that calendering does not significantly affect rate performance in the porosity range. The rate performance is worsened when the electrode is compressed down to less than 20% porosity. A significant loss of rate capability for the electrode from 30% to 0% is observed. At C/2 rate, the electrode at 30% porosity retained 95% of its capacity whereas the electrode at 0% porosity delivered only 50% of its capacity. It is thus concluded that calendering affects rate performance of the electrode, especially when the electrode is pressed to extremely low porosity.

To explain the effects of calendering on rate performance of the $Li[Ni_{1/3}Mn_{1/3}Co_{1/3}]O_2$ cathodes, electrochemical impedance spectroscopy (EIS) was carried out in three electrode cells. Impedance is a collective response of kinetic processes that respond at different time regimes. Nyquist plots of the electrodes at different porosities are presented in Fig. 8. The high frequency intercept with the abscissa refers to the total amount of ohmic resistance of the cell, particularly electrolyte resistance. This resistance is very small compared to the other contributions of resistance for all of the laminates. All the diagrams show two semicircles as the sweep lower frequencies progressed. Some authors assign the high-to-mid-frequency semicircle, referred to as R_e, to the surface film or SEI film formed on the cathode [15–17]. According to our experience, it is most probably associated with the active material particle-to-particle interfacial contact resistance because it is significantly affected by the physical property of the electrode, including the chemical composition, electronic conductivity and porosity [18,19].

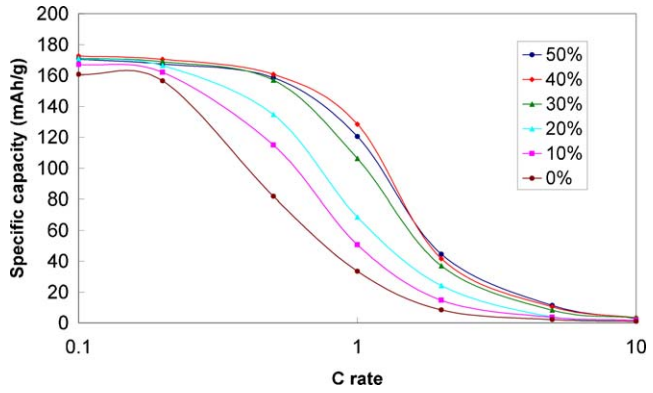

Fig. 7. Rate capability of the $Li[Ni_{1/3}Mn_{1/3}Co_{1/3}]O_2$ cathode at different porosities.

The semicircle in the mid-to-low-frequency range, referred to here as R_{ct}, is believed to be a measure of the charge-transfer resistance at the electrolyte/electrode interface [20,21]. The sloping line at the lowest frequencies, referred to here as R_d, is accepted to be attributed to the diffusion of lithium ions within the electrode [18–21].

As can be seen in Fig. 8, a considerable difference in the high-to-mid-frequency semicircle is observed. From the free standing to the 30% porosity sample, the impedance associated with the active material particle-to-particle interfacial contact resistance drops considerably. After which, the impedance appears to level off. This result suggests that the electrode of high porosity is not very compact and requires a certain degree of compression. This result also tends to support the argument that this resistance in the high-to-mid-frequency region is related to the particle-to-particle contact. If it is ascribed to the SEI resistance, there should be a significant impedance decrease at 0% porosity as the SEI formation reaction is greatly reduced as shown in Fig. 5. The charge transfer resistance, R_{ct}, corresponding to the mid-to-low-frequency semicircle, shows a reverse trend with calendering. Between 50 and 30% porosity, R_{ct} stayed relatively constant with calendering. Further decrease of electrode porosity induces an increase of the charge transfer resistance. From 50% to 0% porosity, R_{ct} almost doubled. The R_{ct} increase is believed to be associated with the interaction between the PVDF/acetylene black composite and the active material particles. With calendering, the PVDF/acetylene black composite is squeezed and fills interstitial space between the active material particles. The electronic path is not damaged in the process since acetylene black is evenly distributed in the composite. However, the ionic path can be blocked when the active material particles are directly covered with the inactive material composite at extremely low porosity. As a non-conductive binder, PVDF has a lithium-ion blocking effect, which hinders lithium ion transfer at the electrode/electrolyte interface [9,22].

Lithium ion transfer at the electrode/electrolyte interface is believed to be the rate-determining step for lithium insertion and de-insertion process. The R_{ct} rise at low porosity range is consistent with the loss of rate capability for the electrode. What is the more, R_d shows a similar trend as R_{ct} with decreasing electrode porosity. A considerable increase from 30% down to 0% porosity is observed. This indicates that lithium diffusion within the electrode is blocked when the electrode is calendered down to a very low porosity. At extremely low porosity, tortuosity of the electrode increases as the pores are filled with inactive materials, which hinder the migration and diffusion of Li ion within the electrode [4,23]. The simultaneous increase of R_{ct} and R_d accounts for the poor rate capability of the

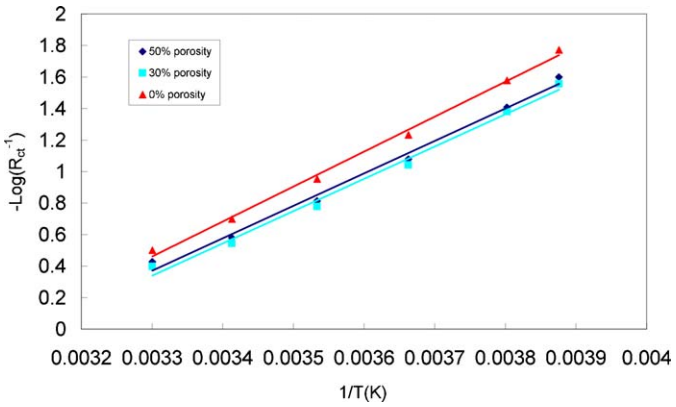

Fig. 9. Temperature dependence of charge transfer resistance at the electrode/electrolyte interface.

electrode at extremely low porosity. A minimum overall resistance ($R_e + R_{ct} + R_d$) is obtained at around 30–40% porosity for the electrode. This is consistent with the relatively high rate performance of the laminate at 30–40% porosity as depicted in Fig. 3.

The charge transfer resistance is known strongly dependent on the ambient temperature. Shrinkage of the semicircle in the middle frequency region with increasing temperature exhibits the decrease of the charge transfer resistance between the $Li[Ni_{1/3}Mn_{1/3}Co_{1/3}]O_2$ electrode and the electrolyte. The activation energy values for the electrode with 50%, 30%, and 0% porosities were evaluated from the temperature dependence of the charge transfer resistances for the electrode at different porosities. Good linearity of the Arrhennius plot between $1/R_{ct}$ and $1/T$ is observed as shown in Fig. 9. The apparent activation energy of the charge transfer is calculated from the angle of each plot. As a result, 39.2, 38.7, and $42.4 \pm 2\,kJ\,mol^{-1}$ were obtained for the electrode at 50%, 30%, and 0% porosities, respectively. The values obtained in this work are comparable with the reported activation energy of lithium ion transfer at the interface of $LiMn_2O_4$, $LiFePO_4$ and other different active materials [24–27]. From 50% to 30% porosity, activation energy for Li interfacial transfer is not considerably changed. This is identical with the fact that the R_{ct} is not considerably affected by calendering from 50% to 30% porosity as discussed above. An increase of the activation energy is obtained when the electrode is squeezed down to 0% porosity. The activation energy increase implies that a high barrier exists for lithium ion transfer at the interface between the cathode and the electrolyte. As the matter of fact, any factors hindering the mobility of lithium ion at the interface contribute to activation energy increase [26,27]. By calendering, PVDF binder fills interstitial space between the active material particles and even covers the active material particle surfaces, which makes lithium-ion transfer at the electrode/electrolyte interface more difficult. This is a reason responsible for the increase of activation energy for Li interfacial transfer. The relatively high activation energy is in agreement with the poor rate capability of the electrode at 0% porosity.

4. Conclusion

Calendering effects on the physical and electrochemical properties of the $Li[Ni_{1/3}Mn_{1/3}Co_{1/3}]O_2$ cathode laminate containing 8% PVDF and 7% acetylene black were investigated. The results show that proper calendering is important for manufacturing $Li[Ni_{1/3}Mn_{1/3}Co_{1/3}]O_2$ composite laminate of high performance. Calendering improves the breaking stress of the laminate whereas the brittleness is simultaneously increased. Meanwhile, another compromise between specific capacity and first coulombic efficiency is obtained. With decreasing electrode porosity, an increase of the first coulombic efficiency is ascribed to the decrease of the specific area of the electrode. However, a decrease of specific capacity is obtained at extremely low porosity. Rate capability of the electrode is also affected by calendering. Poor rate performance of the electrode at extremely low porosity can be explained by the lithium-ion blocking effect of PVDF binder at the electrode/electrolyte interface and the resultant high activation energy for Li interfacial transfer. Taking all the factors into consideration, an optimized porosity of 30–40% for the electrode is identified. It should be noted that the optimized porosity obtained in this study is specific to the categories of active and inactive materials and the electrode composition adopted. Although the results were obtained with thick electrodes of high active material loadings, the trend must be universal for thinner electrode with the same chemical compositions. The results are helpful in optimizing electrode porosity and fabricating electrode of high performance.

Acknowledgment

The authors are greatly indebted to the funding of Natural Science Foundation of China (NSFC, contract no. 21073129).

References

[1] Y.-H. Chen, C.-W. Wang, X. Zhang, A.M. Sastry, J. Power Sources 195 (2010) 2851–2862.
[2] H. Zheng, G. Liu, X. Song, P. Ridgway, S. Xun, V.S. Battaglia, J. Electrochem. Soc. 157 (2010) A1060–A1066.
[3] J. Shim, K.A. Striebel, J. Power Sources 119–121 (2003) 934–937.
[4] I.V. Thorat, D.E. Stephenson, N.A. Zacharias, K. Zaghib, J.N. Harb, D.R. Wheeler, J. Power Sources 188 (2009) 592–600.
[5] L. Liu, N. Zhang, K. Sun, T. Yang, J. Phys. Chem. Solids 70 (2009) 727–731.
[6] I. Belharouak, Y.-K. Sun, J. Liu, K. Amine, J. Power Sources 123 (2003) 247–252.
[7] X. Liu, G. Zhu, K. Yang, J. Wang, J. Power Sources 174 (2007) 1126–1130.
[8] K. Amine, J. Liu, I. Belharouak, S.-H. Kang, I. Bloom, D. Vissers, G. Henriksen, J. Power Sources 146 (2005) 111–115.
[9] G. Liu, H. Zheng, S. Kim, Y. Deng, A.M. Minor, X. Song, V.S. Battaglia, J. Electrochem. Soc. 155 (2008) A887–A892.
[10] G. Liu, H. Zheng, A.S. Simens, A.M. Minor, X. Song, V.S. Battaglia, J. Electrochem. Soc. 154 (2007) A1129–A1134.
[11] L. Wang, Y. Yu, P.C. Chen, D.W. Zhang, C.H. Chen, J. Power Sources 183 (2008) 717–723.
[12] K. Hayashi, Y. Nemoto, S. Tobishima, J. Yamaki, Electrochim. Acta 44 (1999) 2337–2343.
[13] H. Zheng, Y. Fu, H. Zhang, T. Abe, Z. Ogumib, Electrochem. Solid-State Lett. 9 (2006) A115–A119.
[14] D.Y.W. Yu, K. Donoue, T. Inoue, M. Fujimoto, S. Fujitani, J. Electrochem. Soc. 153 (5) (2006) A835–A839.
[15] M.D. Levi, D. Aurbach, J. Phys. Chem. B 101 (1997) 4641–4647.
[16] E. Barsoukov, J.H. Kim, C. Oh Yoon, H. Lee, J. Electrochem. Soc. 145 (1998) 2711–2717.
[17] Y.-G. Ryu, S.-I. Pyun, J. Electroanal. Chem. 433 (1997) 97–105.
[18] H. Zheng, G. Liu, X. Song, V. Battaglia, ECS Trans. 11 (2008) 1–9.
[19] H. Zheng, K. Jiang, T. Abe, Z. Ogumi, Carbon 44 (2006) 203–210.
[20] C. Wang, A.J. Appleby, F.E. Little, J. Electroanal. Chem. 497 (2001) 33–46.
[21] A. Funabiki, M. Inaba, Z. Ogumi, S. Yuasa, J. Otsuji, A. Tasaka, J. Electrochem. Soc. 145 (1998) 172–178.
[22] S. Babinec, H. Tang, A. Talik, S. Hughes, G. Meyers, J. Power Sources 174 (2007) 508–514.
[23] J.-F. Cousseau, C. Siret, P. Biensan, M. Broussely, J. Power Sources 162 (2006) 790–796.
[24] N. Nakayama, T. Nozawa, Y. Iriyama, T. Abe, Z. Ogumi, K. Kikuchi, J. Power Sources 174 (2007) 695–700.
[25] I. Yamada, T. Abe, Y. Iriyama, Z. Ogumi, Electrochem. Commun. 5 (2003) 502–505.
[26] Y. Yamada, Y. Iriyama, T. Abe, Z. Ogumi, Langmuir: ACS J. Surf. Colloids 25 (2009) 12766–12770.
[27] M. Takahashi, S. Tobishima, K. Takei, Y. Sakurai, Solid State Ionics 148 (2002) 283–289.